



The effects of printing parameters on quality, strength, mass, and processing time of polylactic acid specimens produced by additive manufacturing

Carmita Camposeco-Negrete¹ · Julio Varela-Soriano² · José Jorge Rojas-Carreón²

Received: 30 November 2020 / Accepted: 11 June 2021 / Published online: 20 June 2021
© The Author(s), under exclusive licence to Springer Nature Switzerland AG 2021

Abstract

Additive manufacturing (AM) is a technology adopted in numerous industries for rapid prototyping and fabrication. One of the AM technologies is Material Extrusion (ME), according to ISO/ASTM 52,900 standard. Polylactic acid (PLA) is a thermoplastic employed in most of the low-cost 3D printers. Owing to its widespread use, it is fundamental to understand the relationship that exists among the quality of parts made of PLA produced by ME, their mechanical properties as well as their mass and processing time, considering novel infill patterns proposed by various slicer software. This paper proposed an experimental study to optimize these variables by modifying three key parameters (infill pattern, build orientation, and infill percentage) in 3D printing of PLA. The effects of these parameters are analyzed using the Taguchi Methodology and an analysis of variance (ANOVA). A desirability analysis was employed to obtain a set of parameters that allowed the best trade-off among all the variables.

Keywords Material extrusion · 3D printing · Optimization

1 Introduction

Additive manufacturing (AM) processes produce end-use solid objects by stacking layers made of different types of materials. That technology provides benefits when compared to traditional manufacturing, including the avoidance of costing tooling for fabricating the parts [1, 2].

In recent years, it is used for producing parts that are economically viable and robust. By 2025, the annual impact of the market related to AM will be on the order of US\$230 billion to \$550 billion. 3D printing technologies are defining

how to design and manufacture products, and its scope is gradually increasing to cover a large variety of goods [3]. It is attractive to use AM because diverse components have complex geometries or intricate features that cannot be created using traditional manufacturing methods. Additionally, for low production volumes, 3D printing seems an excellent alternative for having profitable parts [4].

One of AM branches is material extrusion (ME), commonly known as fused deposition modeling (FDM) due to the name given by Stratasys. ME is one of the most widely adopted AM technologies due to its low cost regarding materials and maintenance, easy operation, and user-friendliness [5]. In ME, a filament is heated and pressed downwards using a nozzle. The nozzle moves in the XY-plane to create a layer, and then it is displaced along the Z-axis to generate a new layer deposited above the previous one to manufacture a final part [6]. Common materials for FDM are thermoplastics such as acrylonitrile butadiene styrene (ABS), blends of polycarbonate (PC) and ABS, polylactic acid (PLA), polyamide (PA), and poly-ether-ether-ketone (PEEK), among others [7].

Nowadays, there is an increasing number of technologies related to additive manufacturing as well as new materials. Besides, one of the challenges of AM is producing

✉ Carmita Camposeco-Negrete
carmitacamposeco@gmail.com

Julio Varela-Soriano
j.varela@tec.mx

José Jorge Rojas-Carreón
jjrojas@tec.mx

¹ School of Engineering and Science, Tecnológico de Monterrey, Eduardo Monroy Cárdenas 2000, 50110 Toluca, Estado de México, Mexico

² School of Engineering and Science, Tecnológico de Monterrey, Atlixcáyotl 5718, Reserva Territorial Atlixcáyotl, 72453 Puebla, Puebla, Mexico

components that function adequately. PLA is a thermoplastic derived from corn starch or sugar cane. It increases its sustainability and biocompatibility, enabling its usage for medical applications. Additionally, it's a preferred material for ME because it can be printed in a machine without a closed chamber, obtaining parts with good quality and reduced warpage [8].

In AM, printing parameters dictate process outcome. The selection of process parameters influences processing time, quality, and mechanical performance. Layer thickness, infill pattern, infill angle, number of contours, building orientation, height and feed rate of the nozzle, and bed temperature are examples of printing parameters considered in ME. Regarding infill patterns, a few of them are commonly available in most of the slicing software used to prepare parts before sending them for building. New infill patterns granting enhanced mechanical properties or mass reduction are introduced by different software companies. It is critical to explore how they interact with the relevant metrics of ME when printing PLA components, considering other settings, as infill percentage and part orientation, to impart a broader knowledge about infill patterns that can be beneficial for structural applications under tensile loads.

2 Literature review

Several researchers have studied the effects of 3D printing parameters on different responses, using ME and diverse materials.

Hassanifard and Hashemi [6] determined the strain-life fatigue of specimens made of Ultem 9085, polycarbonate (PC), and polylactic acid (PLA). The infill percentage impacted the mechanical properties of printed parts. Verbeeten et al. [9] investigated the strain-rate dependence of yield stress for PLA parts. A modification of the infill angle from 0° to 90° granted anisotropic effects to printed parts.

Chen et al. [10] optimized the manufacturing of PLA army-navy retractors using ME. The strength of parts increased with higher infill percentages, layer thickness and width, and the number of shells. Zhang et al. [11] subjected PLA specimens to tensile tests according to ASTM D638-14 standard. An infill angle of 0° provided the highest tensile strength and dynamic mechanical properties.

Mohamed et al. [12] presented the creep displacement of PC-ABS specimens manufactured by ME. An increased gap reduced part's density. As a result, the structure is brittle, and the material fractures faster. In the work of Zhao et al. [13], the mechanical properties of specimens made of PLA are investigated. Higher values of orientation angle, and smaller ones of layer thickness, raised part's tensile strength.

Yao et al. [14] studied the Ultimate Tensile Strength (UTS) of a part made of PLA. The value of UTS

diminished with a greater layer thickness and a smaller orientation angle. Zhang et al. [15], prognosticated the tensile strength of specimens made of PLA. Layer thickness obtained the highest relevance, followed by the extrude temperature and printing speed. Liu et al. [7] examined the mechanical properties corresponding to wood, ceramic, metal, and carbon fiber PLA composites. The authors reported that the infill and orientation angles have a strong relationship with the mechanical properties of parts.

The aim of the work reported by Gopsill et al. [16] was to optimize the infill structure of a PLA part by topological optimization. The specimen's strength increased when layer thickness diminished. Alafaghani et al. [17] examined mechanical properties and dimensional accuracy of printed pieces made of PLA. Building direction affects dimensional precision considerably. Mohamed et al. [18] investigated the dimensional accuracy of specimens made of a PC-ABS blend. Layer thickness had a major influence on all responses. Raut et al. [19] examined the tensile and flexural behavior, as well as processing time of specimens made of ABS P400. The orientation angle affected the studied variables the most.

Carneiro et al. [20] executed tensile tests using specimens made of polypropylene (PP) and reinforced PP. The layer thickness, infill percentage, and building orientation are the variables of the study. According to the results, the infill percentage has a linear effect on mechanical properties. On the other hand, the layer thickness has a minor influence on tensile behavior. Wu et al. [21] carried out tensile, compressive, and bending trials on PEEK and ABS parts. The authors concluded that layer thickness and infill angle have a large influence on mechanical performance.

Lanzotti et al. [22] modified the values of the layer thickness, infill angle, and the number of contours in 3D printing of ABS samples for executing tensile tests. A large number of contours and an infill angle of 90° achieved higher tensile strength. Alvarez et al. [23] studied the influence of the infill percentage on tensile and impact properties of ABS specimens. The best behavior is achieved using a 100% infill. Christiyan et al. [24] varied the layer thickness and printing speed in 3D printing of ABS coupons for tensile and flexural trials. A small layer thickness and speed provided the best mechanical properties.

Rodriguez-Panes et al. [25] performed tensile tests using PLA and ABS specimens. The layer thickness, infill percentage, and angle are changed to compute their impact. Infill percentage has the highest influence, more noticeable on PLA samples. Camargo et al. [26] printed PLA-graphene coupons for evaluating their mechanical properties when modifying the layer thickness and infill percentage. Both variables have a considerable influence on tensile and flexural behavior.

Terekhina et al. [27] reported a larger tensile strength of nylon coupons when an infill percentage greater than 60% is used. Cerda-Avila et al. [28] found the ultimate tensile stress of PLA coupons is affected by the infill percentage and build orientation. Hanon et al. [29] carried out tensile tests using PLA and high-temperature PLA (HT-PLA) specimens. The best mechanical properties are achieved using 100% infill. Besides, Gawel and Kuciel [30] described a significant impact on mechanical properties caused by the infill percentage.

Researchers have studied the ME process to enhance both the quality and functionality of parts. Nevertheless, no one included in their studies the new patterns offered by processing software. Moreover, most of the investigations presented in this section considered for optimization only the mechanical properties, or a combination of mechanical properties, dimensional precision, cost, and quality, but they did not study all these variables at the same time. A study that considers time, dimensional accuracy, the quantity of material, and mechanical properties for performing optimization of a printed part made of PLA is still missing.

The structural properties of AM parts rely not only on material properties; they are dependent on process parameters used to manufacture a component [31]. Consequently, this research aims to evaluate the effect of three printing parameters (infill pattern, infill percentage, and part orientation) on key metrics related to ME of PLA specimens (processing time, dimensional accuracy, ultimate tensile strength, mass, and strength-to-weight ratio). A multi optimization is performed to obtain a set of parameters that enhance all variables simultaneously.

To print lightweight and profitable parts that exhibit adequate mechanical performance and quality, it's vital to consider the strength-to-weight ratio. The weight of a component impacts its behavior and service life. Companies aim to use the lowest amount of raw material because it reduces costs and environmental impacts. On the other hand, a product must exhibit an acceptable performance based on its strength [32]. Therefore, the strength-to-weight ratio is a relationship used to define a set of parameters that provide the best trade-off between performance and mass.

Finally, all the experimental trials are executed in a low-cost 3D printer. This kind of machine is accessible to almost all users, and its maintenance is relatively easy to perform due to the great variety of information available on the internet. In that fashion, the results provided in this work can be applied by a vast community of consumers interested in improving their components made of PLA, printed using novel infill patterns and affordable 3D printers.

3 Experimental procedure for part's processing using FDM

3.1 Design of the experiment

An L9 array is selected to investigate the effect of printing parameters on the responses (Table 1). Three repetitions are executed in a randomized order for each run of the array. These printing parameters are selected because the articles described in the previous section shown they have the greatest influence on the studied variables.

The S/N ratio is maximized to reduce process variability. For this study, the S/N ratio called “smaller the better” minimizes processing time, part mass, and dimensional deviation. The “larger the better” increases the UTS and the strength-to-weight ratio of the component. Equations 1 and 2 correspond to the S/N ratio “smaller the better” and “larger the better”, respectively.

$$S/N = -10\log\left[(1/n)\left(\sum y^2\right)\right] \quad (1)$$

$$S/N = -10\log\left[\left(\sum (1/y^2)/n\right)\right] \quad (2)$$

3.2 Specimen, material, and 3D printer specifications

The dimensions and geometry of the part are the ones of the Type I specimen of the ASTM D638-14 standard, modeled using NX 11.0 software and exported to STL format. The building material is a silver PLA filament, with a diameter of 1.75 mm, manufactured by ColorPlus. The 3D printer is an ANET A8 (Fig. 1), and Ultimaker Cura 4.3.0 software processes the STL format and set the combination of printing parameters provided by the L9 array.

3.3 Processing time, part's mass, dimensional accuracy, and mechanical properties measurement system

The time is measured with a stopwatch since the extrusion nozzle moves to print the first layer until it returns to its home position once the piece is completed.

Table 1 Factors and their levels

Factor	Level 1	Level 2	Level 3
Infill pattern	Cross 3D	Gyroid	Octet
Orientation angle (°)	0	45	90
Infill percentage (%)	20	50	80

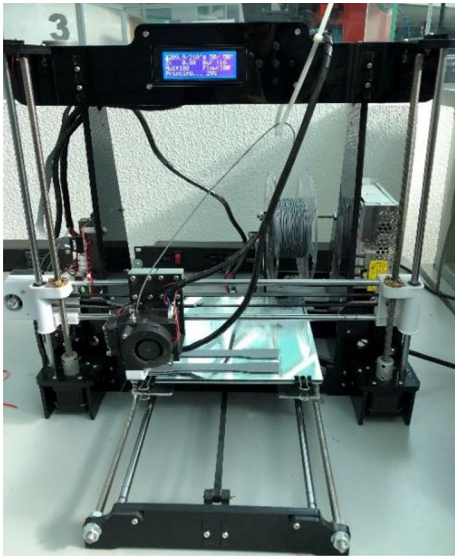


Fig. 1 ANET A8 3D printer

A Shimadzu BW32KH platform balance quantified the mass of each specimen. A Mitutoyo outside micrometer with an accuracy of 0.01 mm determined the length (L), width (W outer and W inner), and thickness (T). Figure 2 shows the measurement locations for each variable. All measures corresponding to the specimen's length were averaged, and the same procedure is applied to the other dimensions.

Dimensional accuracy is calculated as a percentage, using Eq. 3:

$$\Delta D = \left| \frac{D_{\text{EXP}} - D_{\text{DWG}}}{D_{\text{DWG}}} \right| * 100, \quad (3)$$

where ΔD is the deviation between the dimension specified by ASTM D638-14 standard (D_{DWG}), and the one obtained from the printed specimen (D_{EXP}). A greater dimensional accuracy is expected when ΔD is close to zero.

Tensile tests are executed using an Instron machine, at a speed of 1 mm/min (Fig. 3). All data corresponding to

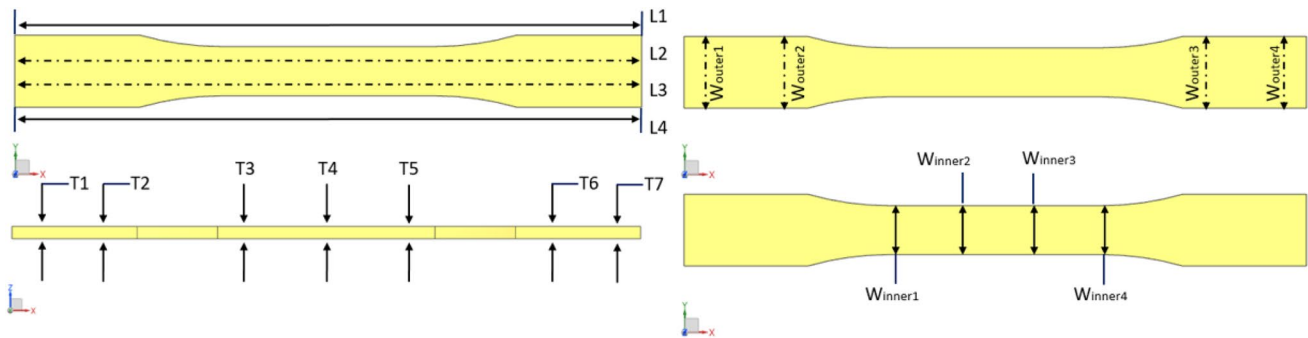


Fig. 2 Measurement locations of the printed part

Fig. 3 From left to right: instron material testing system, and specimen before the test



tensile tests is analyzed using Excel software to determine the ultimate tensile strength (UTS) of each part.

3.4 FDM input process parameters

The layer thickness is set to 0.1 mm for all the parts since this parameter, when lowered, increases the structural integrity of printed pieces [13, 14, 16, 17, 31]. Figure 4 shows the position of specimens when printed.

3.4.1 Infill pattern

In this work, patterns shown in Fig. 5 are chosen because they differ from the most common ones provided by almost all processing software (grid, lines, triangles, zig-zag, among others). Moreover, gyroid and octet patterns use an infill change with every layer to grant a more even distribution of strength over each direction.

3.4.2 Orientation angle

It corresponds to the angle at which the part is placed on the building surface. For the experimental runs, the orientation angle is equal to 0, 45, and 90° (Fig. 5).

3.4.3 Infill percentage

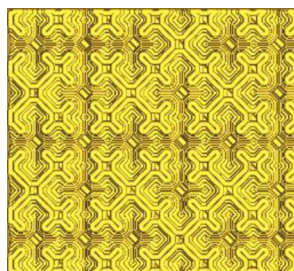
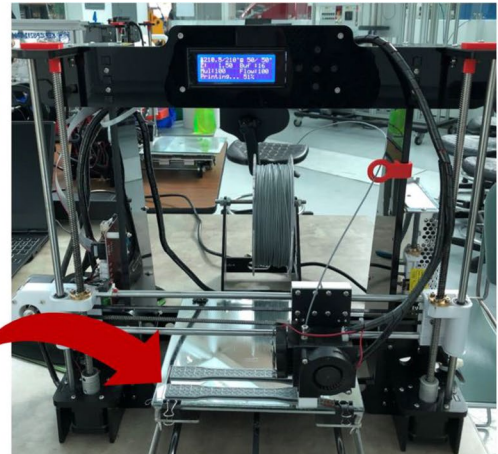
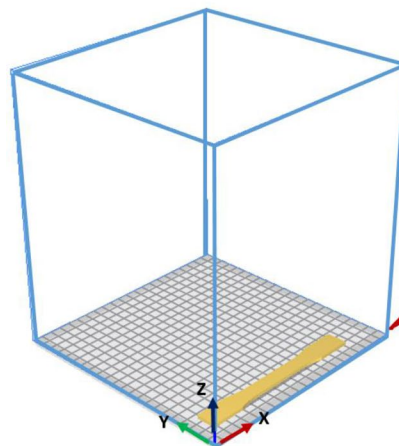
This variable adjusts the infill density of the print. Figure 6 presents three different values taken for this study: 20, 50, and 80%.

4 Results and data analysis

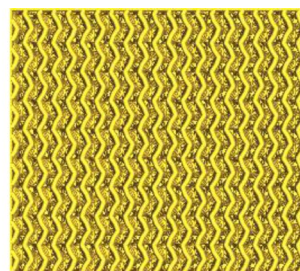
Table 2 presents the results achieved for processing time, dimensional deviation (ΔW_{outer} , ΔW_{inner} , ΔL , and ΔT), specimen’s mass, UTS, and strength-to-weight ratio. Figures 7 and 8 show means analysis, and Figs. 9 and 10 display S/N ratio analysis. In each one of the figures, the dotted line called “A” represents the infill pattern, “B” is the orientation angle, and “C” is the infill percentage. An analysis of variance (ANOVA) and an F test are performed to establish the significance of each factor, considering a confidence level of 95% (Table 3).

As stated by the main effects plot for processing time (Fig. 7a), the lowest time corresponds to the octet infill pattern, with a density of 20%, and the piece oriented at 90°. The infill pattern and infill percentage are the parameters that affect printing time the most (Table 3). As concluded

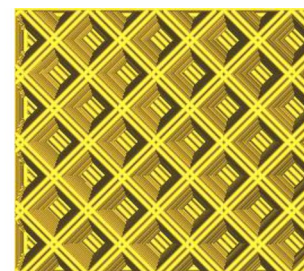
Fig. 4 Position of the specimen on the build platform



Cross 3D



Gyroid



Octet

Fig. 5 Filling patterns preferred for experimental runs

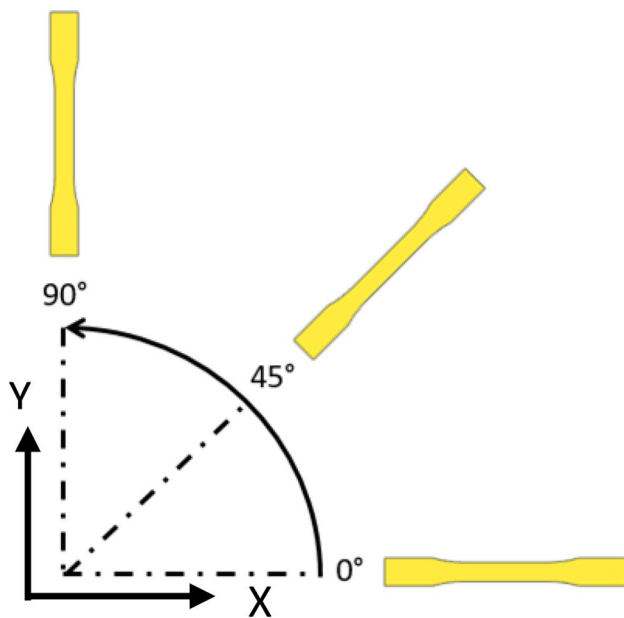


Fig. 6 Orientation angles selected for the experimental trials

by previous works [10, 33, 34], a higher infill percentage increases processing time due to the larger quantity of material extruded to build the part.

The accuracy of dimensions is linked to printing parameters since they impact the development of residual thermal stresses. During a material deposition in 3D printing, thermal gradients appear owing to the cooling and reheating cycles created when a new layer is printed above a previous one. Distortion, delamination, cracking, and failure are consequences of residual thermal stresses [35–37]. Also, dimensional variation is associated with the infill pattern. That parameter dictates the deposition strategy of the material. The sequence followed to extrude the filament can cause non-uniform temperature distributions developing geometric distortions [38].

Dimensional variation regarding W_{outer} and W_{inner} diminish using the octet infill pattern with a density of 50%, and the piece oriented at 90° (Fig. 7b, c). The orientation angle and infill percentage are the dominant factors (Table 3). That corresponds to the findings of [17] and [39]. The spacing between filaments is high using an infill percentage of 50%. A larger spacing and a reduced filament width decrease the residual strains, enhancing dimensional accuracy [40, 41].

Length's dimensional deviation reduces employing the cross 3D infill pattern with a density of 80% and placed at 0° on the building platform (Fig. 7d). The orientation angle and infill pattern have the highest contribution (Table 3). An increment of infill percentage raises length's

Table 2 Experimental results obtained in 3D printing of PLA

Run	Time (h)	ΔW_{outer} (%)	ΔW_{inner} (%)	ΔL (%)	ΔT (%)	Specimen's mass (g)	UTS (MPa)	Strength-to-weight ratio (MPa/g)
1	1.23	3.58	3.58	0.06	3.53	6.53	17.17	2.63
2	1.33	0.51	0.44	0.33	4.46	7.04	17.19	2.44
3	1.50	0.04	1.12	0.32	8.66	7.37	17.96	2.44
4	1.42	1.00	1.79	0.15	3.66	7.54	16.81	2.14
5	1.62	2.07	2.60	0.80	7.10	8.29	17.40	2.20
6	1.23	0.26	0.54	1.48	8.44	5.73	6.62	1.04
7	1.47	1.34	2.04	0.06	4.42	8.79	16.65	1.89
8	1.22	0.30	0.35	0.39	5.94	6.39	19.50	3.05
9	1.35	0.05	0.00	1.55	7.23	6.92	13.25	1.94

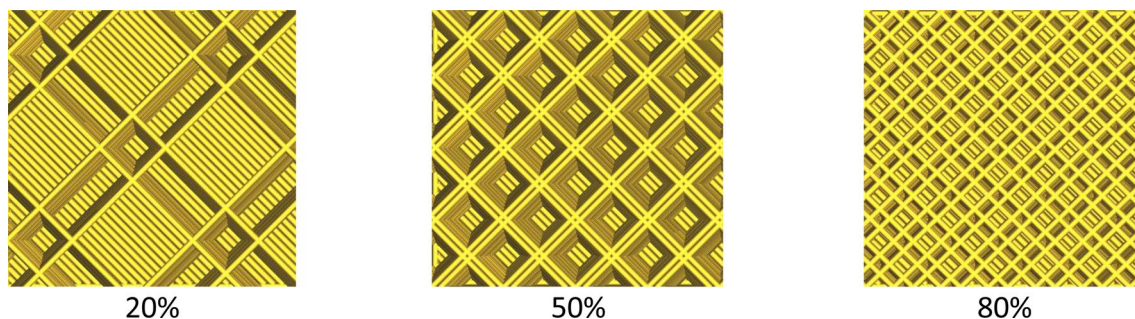


Fig. 7 Infill percentage for octet pattern, oriented at 0° on the printing platform

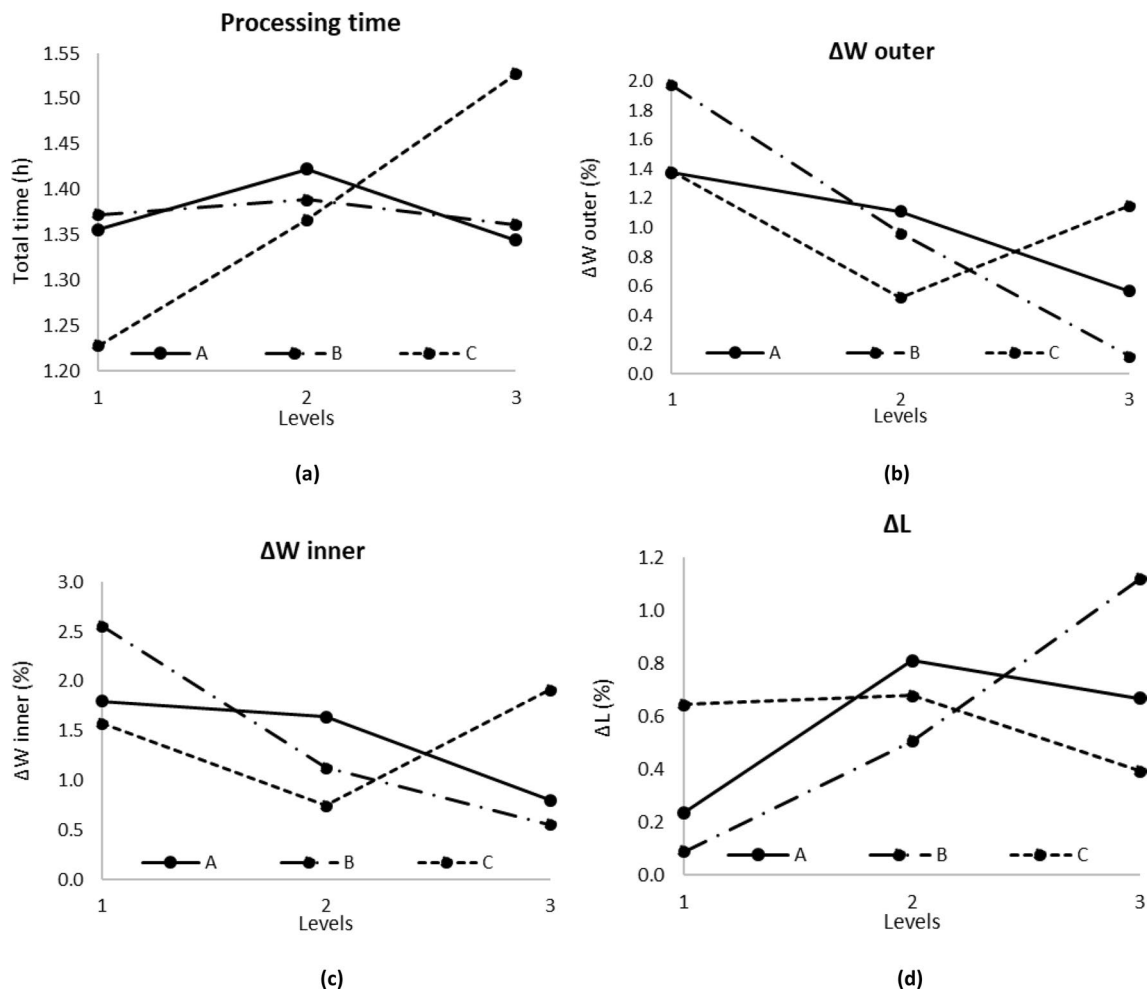


Fig. 8 Mean effects plot for **a** processing time, **b** ΔW_{outer} , **c** ΔW_{inner} , and **d** ΔL

variation [39]. Figure 11 shows a correlation of the three infill patterns analyzed, with a density of 80%, and an orientation angle equal to zero degrees.

The gyroid pattern obtained the highest dimensional deviation (Fig. 7d). As presented in Fig. 11, it has a smaller quantity of empty spaces. When design lines are closer, heat dissipates slowly, and it creates a distorted geometry. When voids are narrow, residual strain increases, affecting dimensional accuracy [40].

Thickness dimensional exactness is enhanced when the cross 3D pattern is used with an infill percentage of 50% and the part orientation equal to 0° (Fig. 8a). The orientation angle and infill percentage are the most significant factors (Table 3). The octet pattern has several overlapped lines that increment the quantity of material at those points. Therefore, octet and gyroid pattern dissipates heat slower, thus increasing thickness' dimensional deviation (Fig. 12). These findings are consistent with [40, 41] since a higher separation between filaments decreases residual strains.

Specimen's mass is minimized using the cross 3D infill pattern with a 20% of infill percentage, and the piece oriented at 90° (Fig. 8b). The two predominant factors are the orientation angle and the infill percentage (Table 3). The cross 3D pattern has a higher quantity of empty spaces, reducing the amount of material used to print the part (Fig. 13).

Lastly, UTS is maximized using the cross 3D infill pattern with an infill percentage equal to 80, and the part at 45° (Fig. 8c). Orientation and infill pattern are the factors that influence the UTS (Table 3). According to Fig. 8c, UTS is higher when the infill percentage is larger since smaller void sizes enhance the part's strength [6, 10, 12, 17, 31, 33, 42]. Additionally, a large infill percentage raises the strength of printed parts because more material is used to build a component, providing better stability [43–45].

The orientation of the part has an important role in the mechanical properties of 3D printed components, as stated by Table 3 and several authors [7, 13, 14, 16, 31]. When the alignment of infill is coincident with stress' direction, the

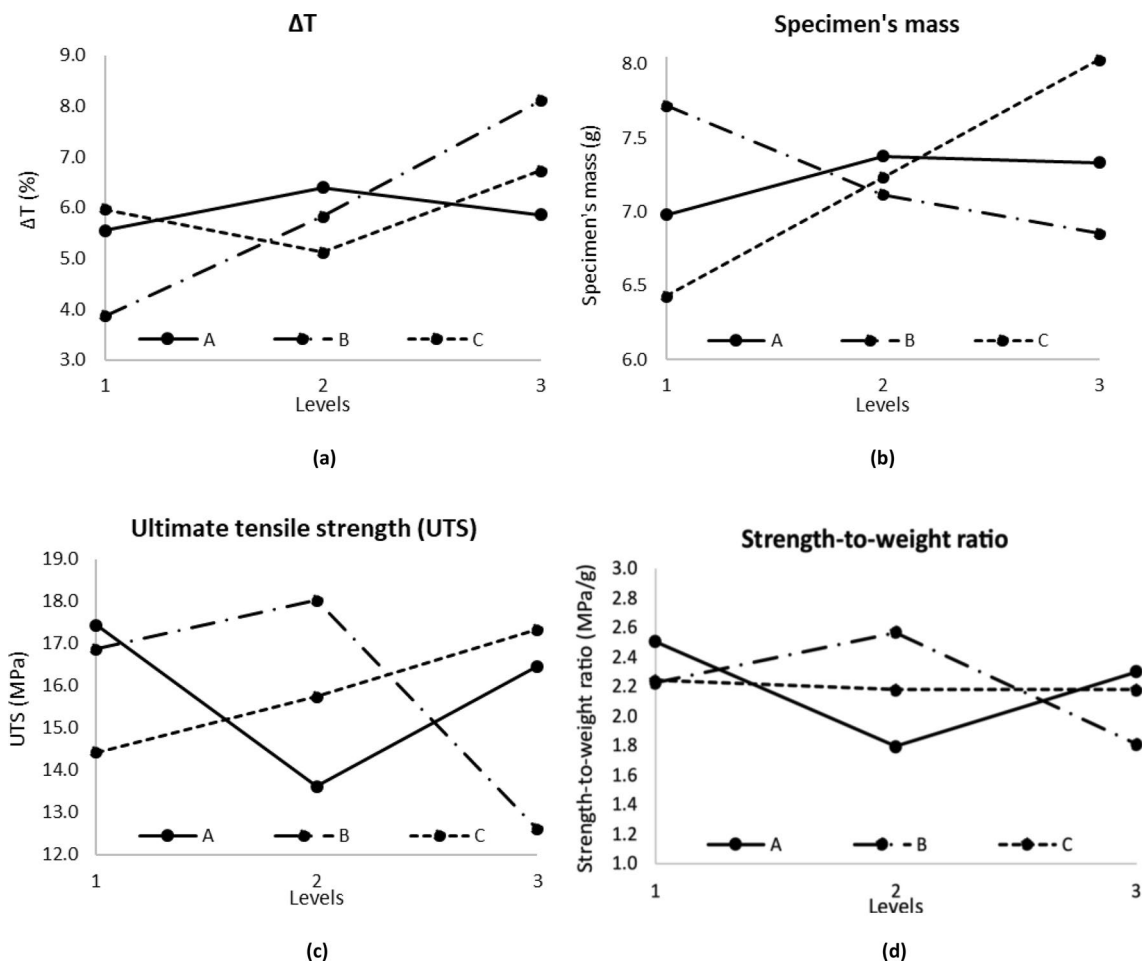


Fig. 9 Mean effects plot for **a** ΔT , **b** specimen's mass, **c** ultimate tensile strength, **d** strength-to-weight ratio

strength of the piece increases [12]. An orientation angle of 45° helps to align infill pattern lines to the direction of stress application, for the case of octet pattern (Fig. 14). Nevertheless, that pattern has a higher number of lines perpendicularly oriented than the ones parallel to stress' direction. The gyroid pattern has no coincident lines to the direction of force applied, for a 45° orientation angle. On the other hand, for cross 3D pattern, the infill percentage used provides a high quantity of material, thus decreasing void sizes and raising part's mechanical strength. The orientation at 45° is coincident with the conclusions presented by [46].

As mentioned in Sect. 2, the strength-to-weight ratio determines the best relationship between performance and mass. The higher the value of that ratio, the lighter and stronger the component will be. As shown in Fig. 8d, the strength-to-weight ratio increases using a cross 3D pattern oriented at 45° with an infill density of 80%. These values are coincident with the ones for enhancing the UTS. From Fig. 14, it can be appreciated that the cross 3D pattern provides a balance between strength and quantity of material since its deposition strategy contains an adequate number of

voids that reduce material consumption without affecting the strength of the specimen.

Figures 9 and 10 present S/N ratio plots for all the factors studied. According to these figures, the levels of infill pattern, orientation angle, and infill percentage that optimize the responses are the same as the ones that reduce process variation. Specimens corresponding to first iteration of the L9 array, before and after the execution of tensile tests, are found in Fig. 15.

Regarding the fracture mode (Fig. 15), samples 1, 2, 4, and 6 broke along the direction of the deposited filaments. The infill percentage for all specimens is lower than 100%. Therefore, porosity is present and is related to a loss of mechanical properties. Moreover, from that figure, delamination and bonding issues happened during testing, altering the maximum UTS reached by coupons.

Specimens 3, 5, 7, 8, and 9 have a fracture perpendicular to the loading direction. According to Table 2, specimen 8 possesses the highest average value for UTS. As reported by [47], its type of fracture is linked to pattern failure instead of delamination and bonding issues. Moreover, an orientation

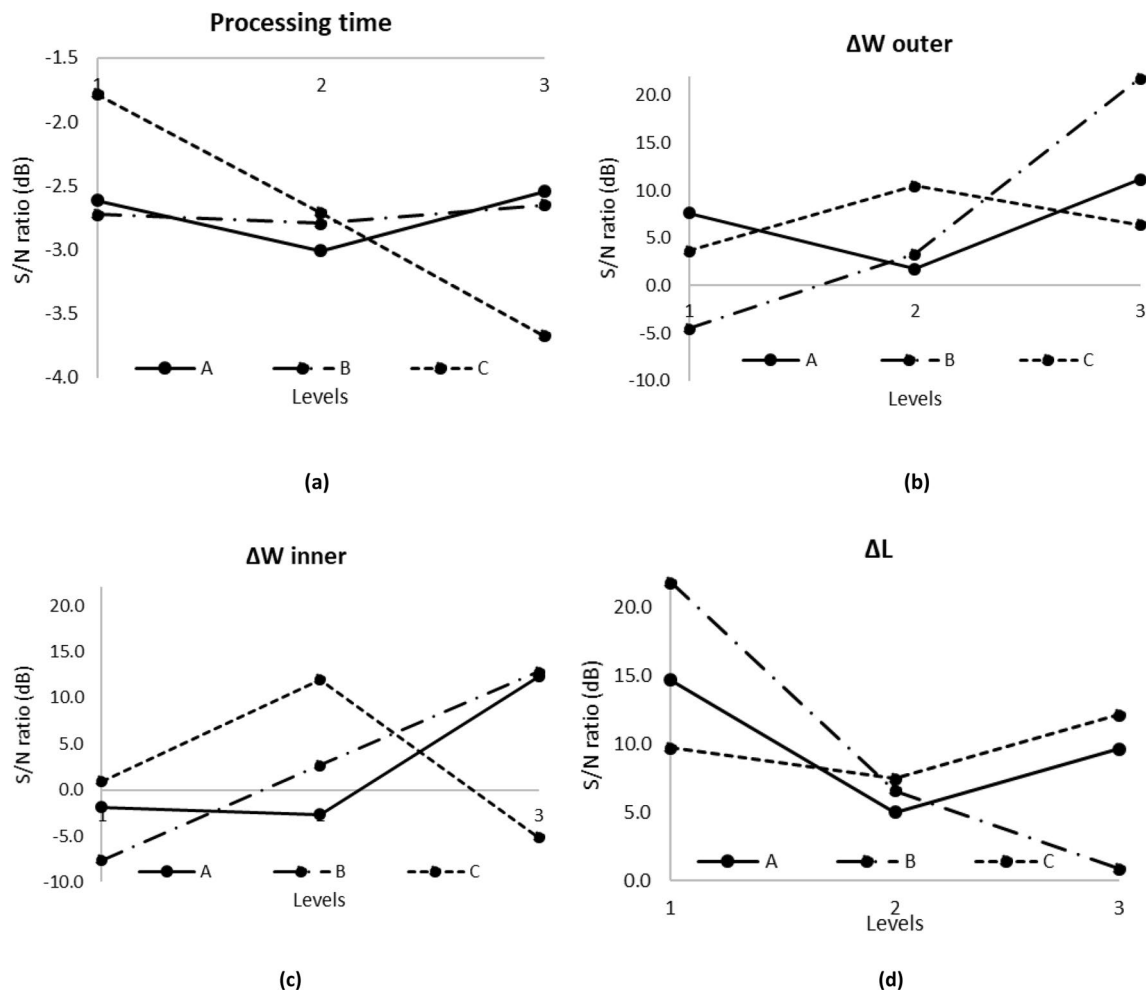


Fig. 10 S/N ratio plot for a processing time, b ΔW_{outer} , c ΔW_{inner} and d ΔL

Table 3 ANOVA–percentage of contribution

Factor	% Contribution							
	Processing time	ΔW_{outer}	ΔW_{inner}	ΔL	ΔT	Specimen’s mass	UTS	Strength-to-weight ratio
Infill pattern	6.96	9.34	3.83	19.88	3.43	5.22	20.25	31.48
Orientation angle	0.87	47.12	51.74	59.43	84.05	21.77	41.75	33.97
Infill percentage	88.98	10.79	44.34	5.37	12.06	70.29	10.85	0.33

angle of 45° enhances UTS (Figs. 8c, 10c). That angle is coincident with the one of specimen 8.

4.1 Multi-optimization for enhancing coupon’s performance and quality for novel infill patterns

Results presented in the previous section showed values of process parameters that enhance one variable are not

necessarily the same for the other ones. It is essential to determine a set of parameters that allows simultaneous optimization of variables. For achieving that, a desirability analysis is executed using Minitab v18. Weight and importance values for the analysis are set to one since both are equally relevant for the solution. Desirability analysis results are in the range from zero to one. A value near or equal to one is useful, and zero means the set of

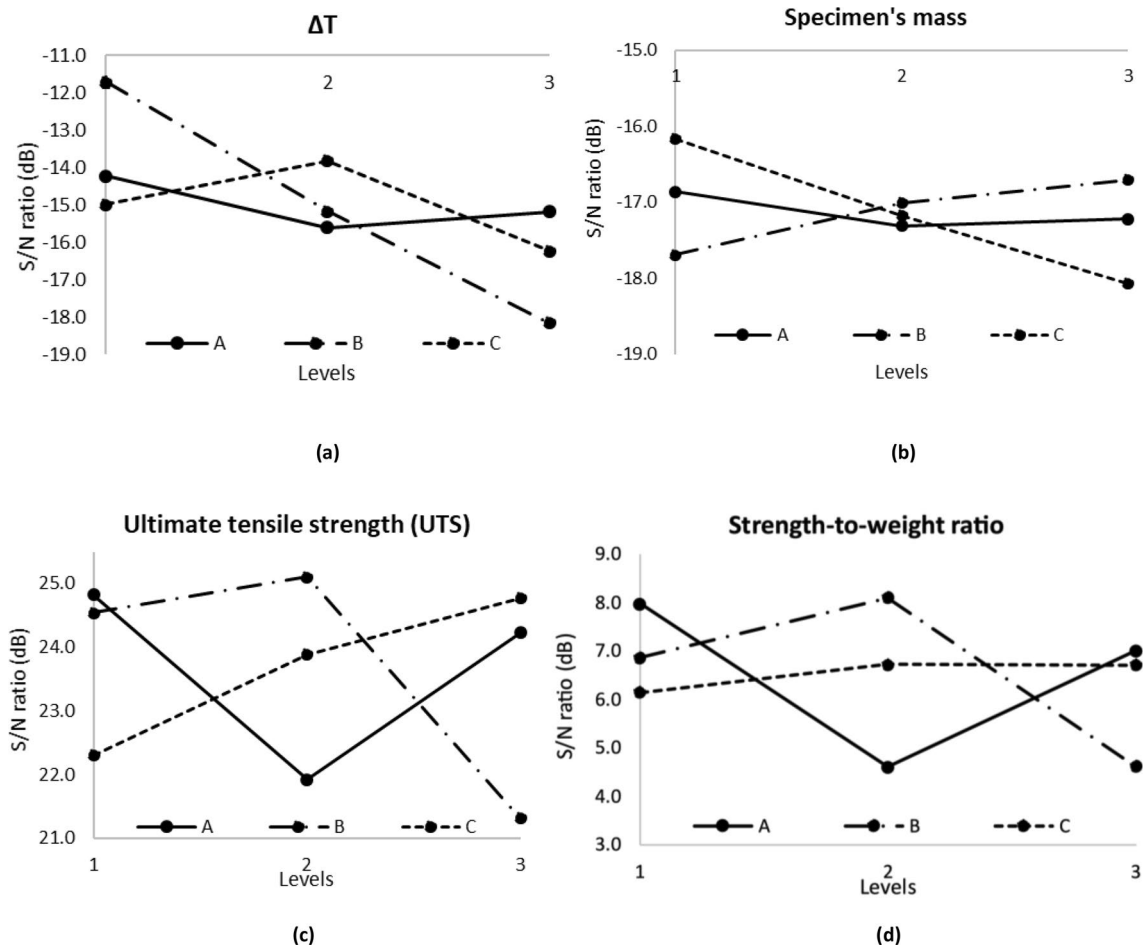


Fig. 11 S/N ratio plot for a ΔT , b specimen's mass, c ultimate tensile strength, d strength-to-weight ratio

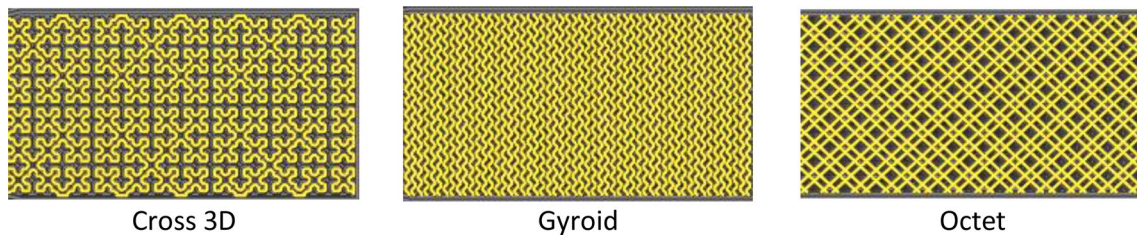


Fig. 12 Comparison among patterns, considering an infill percentage of 80% and part orientation of 0°

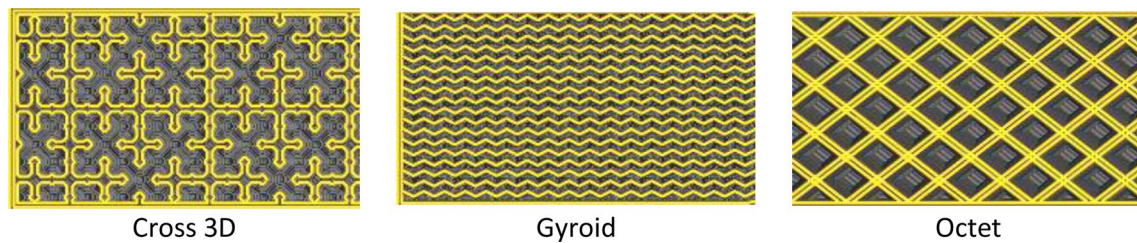


Fig. 13 Comparison among patterns, considering an infill percentage of 50% and part orientation of 0°

Fig. 14 Comparison among patterns, considering an infill percentage of 20% and part orientation of 90°

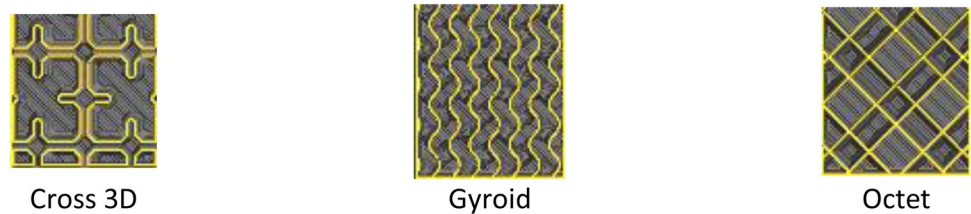


Fig. 15 Comparison among patterns, considering an infill percentage of 80% and part orientation of 45°

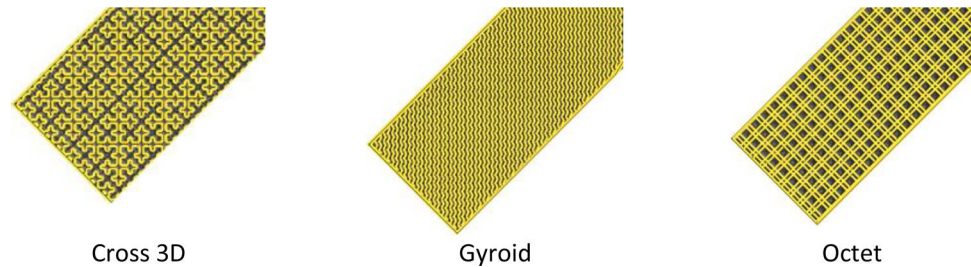


Table 4 Solutions from the desirability analysis

Solution	Infill pattern	Orientation angle (°)	Infill percentage (%)	Desirability value
1	Octet	30	20	0.8764
2	Octet	15	20	0.8491
3	Octet	45	20	0.8452

parameters is not eligible because it does not meet the target. Table 4 presents the desirability analysis' results.

Solution 1 attained the highest value of desirability among the solutions provided by the analysis. Therefore, that set of parameters is the one that optimizes all the variables simultaneously. Three parts were printed using the set obtained from the desirability analysis to corroborate the results given by the study. Table 5 displays the results, and the difference between experimental and predicted values is close to 11% or lower than this percentage.

A multi-optimization often provides the best results for certain variables, while the others are worsened. To

show that, Table 6 offers a comparison between the results obtained using the set of parameters granted by the desirability analysis, and the ones that came from the Taguchi methodology for each variable. Scenario 1 corresponds to desirability analysis' results. Scenarios 2–8 belong to minimum processing time, ΔW_{outer} , ΔW_{inner} , ΔL , ΔT , specimen's mass, and maximum UTS according to Taguchi analysis.

The desirability analysis enhanced outer width's dimensional accuracy, as well as the percentage of deviation corresponding to the specimen's length when compared to the Taguchi methodology. These variables are diminished by 59.76 and 95.64%, respectively. Another variable that is improved using the desirability analysis is the UTS, having a difference equal to 3.24% concerning Taguchi methodology. The set of parameters provided by the desirability analysis did not granted the best results for all the responses, but it allowed to find a good trade-off among the variables for 3D printing of PLA.

Table 5 Results achieved using solution 1 of desirability analysis

Variable	Model prediction	Experimental result	% Difference
Total time (h)	1.20	1.20	0
ΔW_{outer} (mm)	0.37	0.33	- 10.81
ΔW_{inner} (mm)	0.83	0.89	6.75
ΔL (mm)	0.02	0.019	- 7.50
ΔT (mm)	5.54	4.98	- 10.11
Specimen's mass (g)	6.58	6.48	- 1.50
Ultimate tensile strength (MPa)	20.44	21.81	6.71
Strength-to-weight ratio (MPa/g)	3.11	3.37	8.35

Table 6 Comparison between the results achieved using the desirability analysis and the Taguchi methodology

Response	Scenarios								
	1	2	3	4	5	6	7	8	9
Processing time (h)	1.20	1.19							
ΔW_{outer} (mm)	0.33		0.82						
ΔW_{inner} (mm)	0.89			0.72					
ΔL (mm)	0.019				0.42				
ΔT (mm)	4.98					2.66			
Specimen's mass (g)	6.48						5.8		
Ultimate tensile strength (MPa)	21.81							21.13	
Strength-to-weight ratio (MPa/g)	3.37								3.64
Difference between scenarios (%)	–	1.25	– 59.76	23.16	– 95.64	86.97	11.68	3.24	– 7.42

Table 7 DoE for comparative analysis

Factor	Level 1	Level 2	Level 3
Filling pattern	Zigzag	Grid	Tri-hexagon
Orientation angle (°)	0	45	90
Infill percentage (%)	20	50	80

4.2 Comparative analysis for novel and common infill patterns

In Sect. 4.1, a desirability analysis defined the set of printing parameters that enhance all variables simultaneously. The effect of novel infill patterns, infill percentage, and orientation angle of the specimen is studied. Consequently, a comparison between the novel and commonly used deposition strategies is presented.

An L9 array tests typical infill patterns, maintaining the same levels for orientation angle and infill percentage presented in Table 1. Table 7 shows the design of experiments employed for testing three usual infill strategies: zigzag, grid, and tri-hexagon. The experimental results of the L9 array are found in Table 8. Graphs corresponding to means and S/N ratio are exhibited in Figs. 15, 16, 17, 18.

Table 8 Experimental results for common infill patterns

Run	Time (h)	ΔW_{outer} (%)	ΔW_{inner} (%)	ΔL (%)	ΔT (%)	Specimen's mass (g)	UTS (MPa)	Strength-to-weight ratio (MPa/g)
1	0.85	0.39	3.08	1.82	0.00	5.10	12.31	2.41
2	1.00	5.00	6.73	2.12	0.45	6.50	16.04	2.47
3	1.18	0.13	0.38	2.42	0.89	8.20	20.72	2.53
4	1.03	0.13	1.54	2.27	4.46	6.60	13.09	1.98
5	1.18	4.61	8.27	0.98	0.00	7.90	19.96	2.53
6	0.85	3.82	4.62	1.21	4.02	5.10	9.81	1.92
7	1.20	0.53	1.15	1.82	4.02	8.00	16.39	2.05
8	0.83	6.18	7.69	1.14	0.00	4.80	10.08	2.10
9	1.02	3.68	5.19	1.29	0.00	6.20	11.71	1.89

The percentage of contribution for each factor is shown in Table 9.

Moreover, solid specimens printed with orientation angles of 0, 45, and 90° (three repetitions each) are built and tested to complete the comparative analysis and demonstrate the advantages and disadvantages of novel infill patterns. The results of these tests are displayed in Table 10.

According to Figs. 15 and 16, the zigzag infill pattern reduces the processing time, outer and inner width inaccuracy, and thickness dimensional deviation. That pattern increases the UTS and the strength-to-weight ratio. The tri-hexagon infill enhances length accuracy and the specimen's mass. An infill percentage of 20% improves the processing time, length and thickness exactness, and specimen's mass. An 80% of infill increases outer and inner width accuracy, UTS, and the strength-to-weight ratio. Finally, an orientation angle of 45° boosts the processing time, length and thickness accuracy, mass, UTS, and strength-to-weight ratio. A 0° angle corresponds to outer and inner width exactness. Experimental findings coincide with the conclusions shown in [19, 36, 40, 43–45, 48–50]. The signal-to-noise ratio graphs (Figs. 17, 18) show a good agreement with means graphs (Figs. 15, 16). Regarding the percentage of contribution for each factor, the orientation angle has the highest

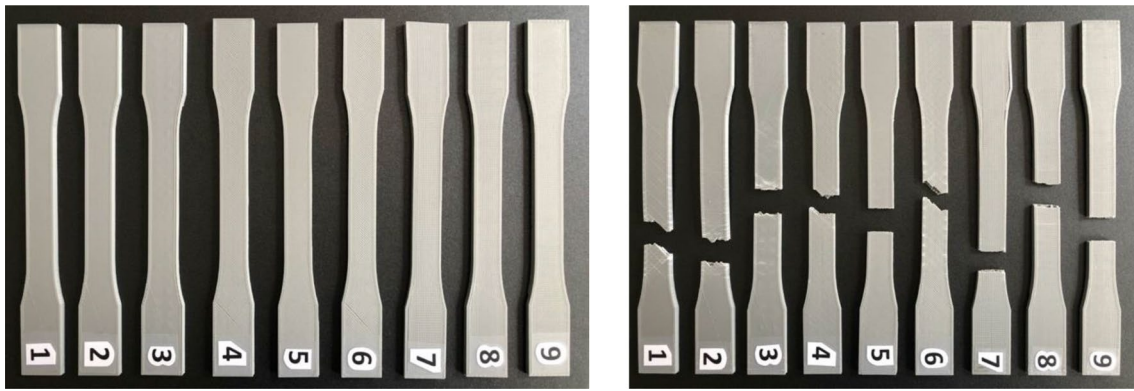


Fig. 16 Specimens before (left) and after tensile tests (right)

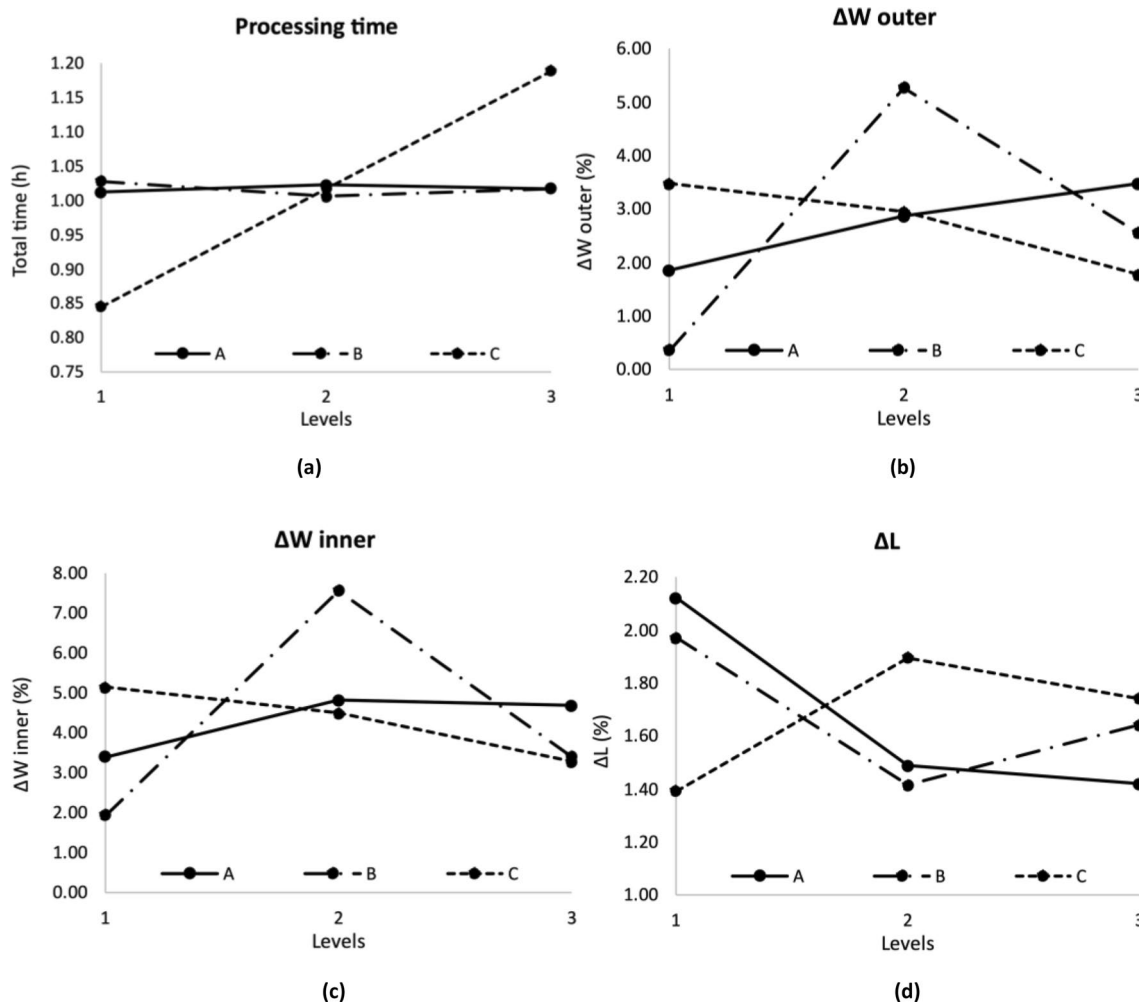


Fig. 17 Mean effects plot for **a** processing time, **b** ΔW_{outer} , **c** ΔW_{inner} , and **d** ΔL

percentage for the dimensional accuracy of outer and inner width and thickness. The infill percentage is relevant for the processing time, mass, and UTS. Lastly, the infill pattern

has the largest contribution for the length exactness and the strength-to-weight ratio.

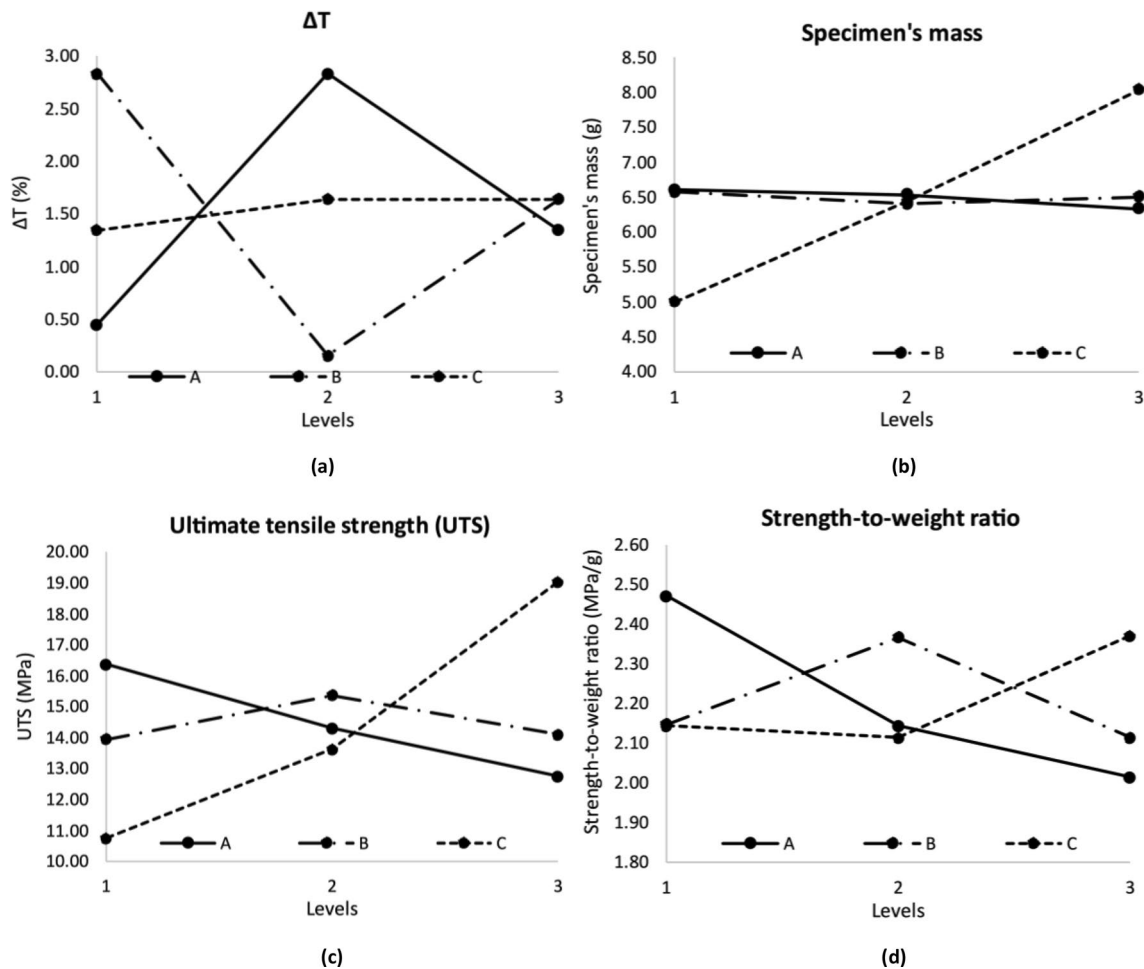


Fig. 18 Mean effects plot for **a** ΔT , **b** specimen's mass, **c** ultimate tensile strength, **d** strength-to-weight ratio

Table 9 ANOVA–percentage of contribution

Factor	% contribution							
	Processing time	ΔW_{outer}	ΔW_{inner}	ΔL	ΔT	Specimen's mass	UTS	Strength-to-weight ratio
Infill pattern	0.08	11.95	9.22	39.01	8.87	0.98	15.64	56.05
Orientation angle	0.47	58.57	43.63	25.43	14.51	0.38	2.62	20.09
Infill percentage	99.42	9.14	24.85	15.63	9.28	98.46	81.42	19.86

Table 10 Experimental results for solid specimens

	Orientation angle ($^{\circ}$)	Time (h)	ΔW_{outer} (%)	ΔW_{inner} (%)	ΔL (%)	ΔT (%)	Specimen's mass (g)	UTS (MPa)	Strength-to-weight ratio (MPa/g)
S1	0	1.32	0.53	3.85	0.91	6.25	8.90	31.97	3.59
S2	45	1.30	6.32	6.92	0.98	6.25	8.80	27.94	3.18
S3	90	1.32	3.95	4.81	1.21	0.00	9.10	22.14	2.43

Novel strategies are printed slower than common patterns. The latter provides higher thickness accuracy and lower mass. On the other hand, novel patterns exhibited elevated UTS values and strength-to-weight ratio for most coupons. Solid specimens and novel strategies take a similar time to be printed. They require a higher quantity of material that affects their thickness dimensional accuracy. Nevertheless, it enhances their UTS since large numbers for that variable are registered. Consequently, coupons display a larger strength-to-weight ratio. Specimens corresponding to the first iteration of the L9 array for common patterns, before and after the execution of tensile tests, are found in Fig. 19. Coupons labeled as S1, S2, and S3 correspond to solid specimens (Table 10).

The fracture pattern is similar to the behavior exhibited by novel strategies. Specimens broke by adhesion issues or by pattern failure. All solid coupons showed fractures generated by pattern failure since porosity is minimized in printed parts with an infill density of 100%. However, thermal stresses develop due to the larger mass of material deposited per layer, weakening the structure (Figs. 20, 21).

4.3 Multi-parameter optimization for commonly used infill patterns

As showed in Sect. 4.1, a desirability analysis is carried out to define a set of printing parameters that maximize printed specimen’s performance, using the levels shown in Table 7. Restrictions and considerations for desirability analysis are available in Sect. 4.1. Results are presented in Table 11.

Solution one provides the largest value of desirability. Consequently, three specimens are printed with the parameters established by that solution to contrast experimental versus predicted values (Table 12). The percentage of difference for all variables is lower than 10%.

A comparison is executed between results obtained from the Taguchi methodology and the desirability analysis (Table 13). As discussed in Sect. 4.1, the multi-optimization values are not the best ones when contrasted to individual optimization carried out by the Taguchi method. The desirability analysis enhances certain variables and worsens others while trying to find the best trade-off among them.

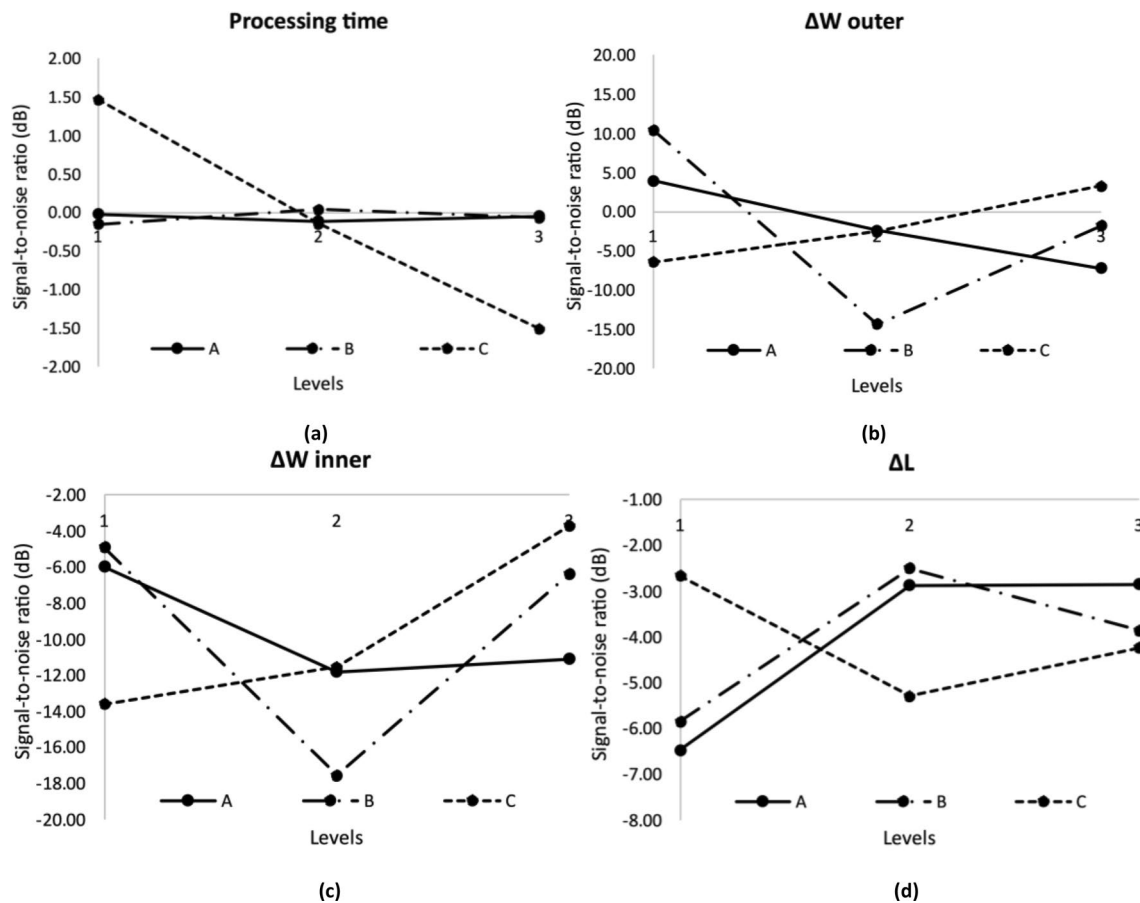


Fig. 19 S/N ratio plot for a processing time, b ΔW_{outer} , c ΔW_{inner} , and d ΔL

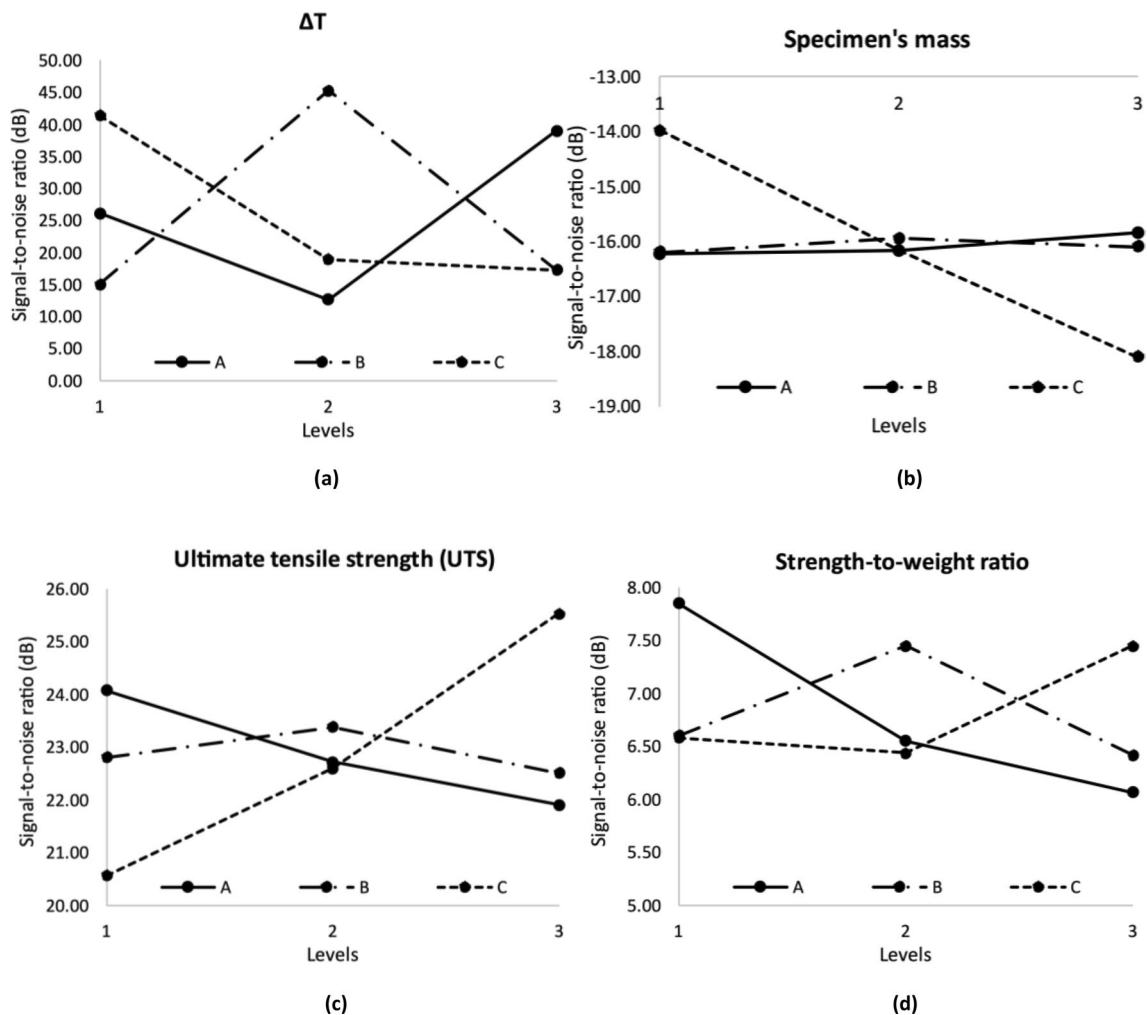


Fig. 20 S/N ratio plot for **a** ΔT , **b** specimen's mass, **c** ultimate tensile strength, **d** strength-to-weight ratio

4.4 Weighing of novel and common infill pattern multi optimization

As stated by the results presented in Sects. 4.1 and 4.3, multi-optimization procedures provide a set of printing parameters used to balance all the specifications (production time, dimensional accuracy, lightweight structure, and superior strength). Comparing the set of parameters for novel and common patterns, the former needs more time to be printed (42.9%), but the dimensional accuracy and the strength-to-weight ratio increase up to 98, and 33% respectively (except for thickness exactness, its best results are linked to a zig-zag pattern). In contrast with solid infill, the octet pattern reduces printing time (reduction of 8.86% compared with S1, which possesses the largest strength-to-weight ratio), a higher dimensional accuracy (improvement of 20–98%), and a mass decrement (27%). On the other hand, solid coupons exhibited larger UTS values than parts printed with the octet pattern (an increase of 32%). Besides, the strength-to-weight

ratio is higher for the solid infill (6.30%). The octet pattern generates light and strong structures with acceptable dimensional accuracy and prints faster than the solid infill (Table 14).

5 Conclusions

An experimental study is executed to enhance different responses related to 3D printing of parts made of PLA, with a focus on novel infill patterns provided by slicer software. These responses are part quality, measured as a percentage of dimensional deviation, processing time, specimen's mass, ultimate tensile strength, and the strength-to-weight ratio to assess the relationship between producing lightweight and strong structures. These responses are associated with different printing parameters. The experiments performed for this work considered the infill pattern, orientation angle, and infill percentage as process parameters.

Fig. 21 Specimens using common infill patterns before (left) and after tensile tests (right)

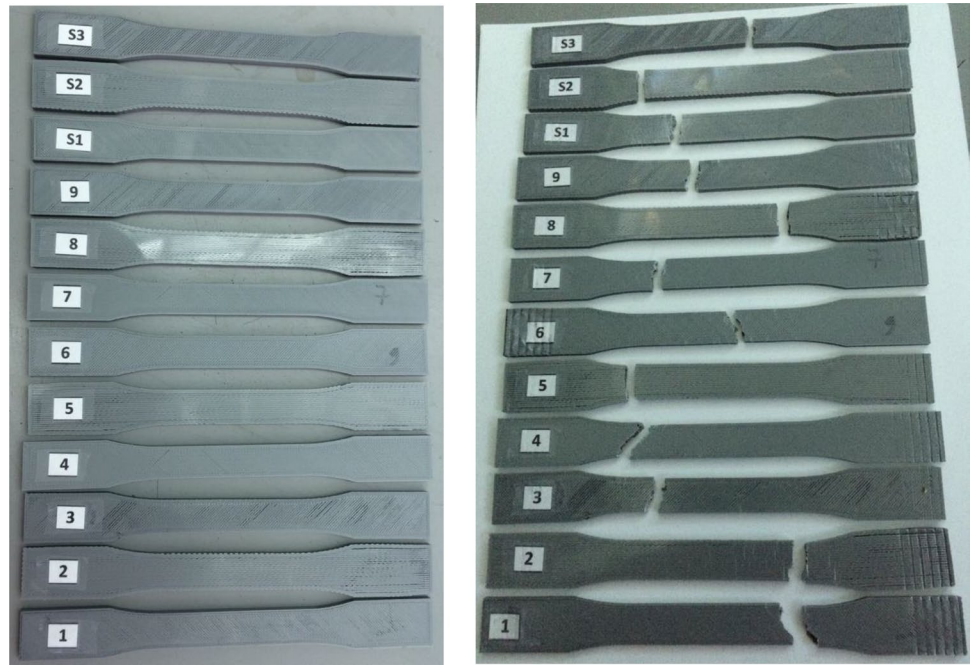


Table 11 Solutions from the desirability analysis for common patterns

Solution	Infill pattern	Orientation angle (°)	Infill percentage (%)	Desirability value
1	Zigzag	90	20	0.6133
2	Zigzag	0	20	0.5819
3	Zigzag	45	20	0.4872

The Taguchi methodology and an analysis of variance are applied to study the effect and influence of printing parameters on responses and determine the parameters with the highest impact. An L9 array defines the design of the experiment, considering three different levels for each printing parameter. Moreover, to compare the novel and common patterns performance, a new experimental design is carried out.

Solid specimens are printed to contrast their characteristics with the ones of common and novel deposition strategies.

The orientation angle and infill percentage impact the width and thickness dimensional accuracy and specimen’s mass of novel patterns. The infill pattern and orientation angle influence length dimensional exactness, ultimate tensile strength, and the strength-to-weight ratio. Infill percentage and infill pattern affect processing time. Concerning common patterns, their outer and inner width and thickness accuracy are affected by the orientation angle. The highest percentage of contribution for the processing time, mass, and UTS correspond to the infill percentage. The infill pattern affects length accuracy and the strength-to-weight ratio.

A desirability analysis is carried out to obtain a set of parameters that support a multi-optimization of all responses. That analysis is executed for common and novel patterns. According to the results, when printing a part using the octet pattern and an infill percentage of 20, with

Table 12 Results achieved using solution 1 of desirability analysis for common patterns

Variable	Model prediction	Experimental result	% Difference
Total time (h)	0.84	0.84	0.00
ΔW_{outer} (mm)	2.41	2.40	- 0.41
ΔW_{inner} (mm)	3.33	3.30	- 0.90
ΔL (mm)	1.80	1.75	- 2.78
ΔT (mm)	0.35	0.34	- 2.86
Specimen’s mass (g)	5.12	5.20	1.56
Ultimate tensile strength (MPa)	12.25	13.10	6.94
Strength-to-weight ratio (MPa/g)	2.39	2.52	5.41

Table 13 Comparison between the results achieved using the desirability analysis and the Taguchi methodology for common patterns

Response	Scenarios								
	1	2	3	4	5	6	7	8	9
Processing time (h)	0.84	0.83							
ΔW_{outer} (mm)	2.40		2.09						
ΔW_{inner} (mm)	3.30			3.22					
ΔL (mm)	1.75				1.87				
ΔT (mm)	0.34					0.31			
Specimen's mass (g)	5.20						4.76		
Ultimate tensile strength (MPa)	13.10							21.83	
Strength-to-weight ratio (MPa/g)	2.52								4.59
Difference between scenarios (%)	–	1.20	14.83	2.48	– 6.42	9.68	9.24	– 39.99	– 45.05

Table 14 Comparison between sets of parameters provided by multi optimization

Variable	Novel patterns	Common patterns	Solid infill (S1)	% Difference between novel and common	% Difference between solid and common
Total time (h)	1.20	0.84	1.32	42.86	– 8.86
ΔW_{outer} (mm)	0.33	2.40	0.53	– 86.25	– 37.30
ΔW_{inner} (mm)	0.89	3.30	3.85	– 73.03	– 76.86
ΔL (mm)	0.02	1.75	0.91	– 98.91	– 97.91
ΔT (mm)	4.98	0.34	6.25	1364.71	– 20.32
Specimen's mass (g)	6.48	5.20	8.90	24.62	– 27.19
Ultimate tensile strength (MPa)	21.81	13.10	31.97	66.49	– 31.78
Strength-to-weight ratio (MPa/g)	3.37	2.52	3.59	33.60	– 6.30

an orientation angle of 30°, attains the best trade-off among the studied variables. These values reduce the length and width dimensional variation. Also, they increase the ultimate tensile strength of the part without a significant increment of both processing time and mass. On the other hand, for common deposition strategies, a zigzag pattern with an infill of 20% and an orientation angle of 90° granted the best desirability value.

When contrasting the octet and zigzag configurations, the octet pattern lasts more in printing, but the dimensional accuracy and the strength-to-weight ratio of specimens are enhanced. The solid infill exhibited larger values of UTS and strength-to-weight ratio than the octet strategy. Nevertheless, the octet pattern reduces the specimen's mass, processing time, and dimensional inaccuracy. Consequently, that strategy is capable of providing sound and lightweight components in less time than solid infill. This study shows novel deposition strategies are a viable alternative to commonly used infill patterns. They incorporate features that allow an enhancement of processing variables. Consequently, research efforts should be conducted to design novel patterns. The objective is to improve the

overall performance of printed specimens using affordable 3D printers to impact a higher number of users.

Acknowledgements The author would like to thank the Tecnológico de Monterrey Campus Puebla for providing the 3D printer and material for conducting the experimental trials. This research did not receive any specific grant from funding agencies in the public, commercial, or not-for-profit sectors.

Author's contributions Carmita Camposeco-Negrete: study conception and design, analysis and interpretation of data, drafting of manuscript, and critical revision. Julio Varela-Soriano: data acquisition, critical revision of manuscript. José Jorge Rojas-Carreón: data acquisition, critical revision of manuscript.

Funding This research did not receive any specific grant from funding agencies in the public, commercial, or not-for-profit sectors.

Data availability The raw/processed data required to reproduce these findings cannot be shared at this time as data also form part of an ongoing study. The datasets generated during and/or analyzed during the current study are not publicly available as data also form part of an ongoing study but are available from the corresponding author on reasonable request.

Declarations

Conflict of interest The authors declare that they have no known competing financial interests or personal relationships that could have appeared to influence the work reported in this paper.

Code availability. Not applicable.

References

- Conway KM, Pataky GJ (2019) Craze in additively manufactured acrylonitrile butadiene styrene. *Eng Fract Mech* 211:114–124. <https://doi.org/10.1016/J.ENGFRACMECH.2019.02.020>
- Alaimo G, Marconi S, Costato L, Auricchio F (2017) Influence of meso-structure and chemical composition on FDM 3D-printed parts. *Compos Part B Eng* 113:371–380. <https://doi.org/10.1016/J.COMPOSITESB.2017.01.019>
- Manyika J, Chui M, Bughin J, et al Disruptive technologies: Advances that will transform life, business, and the global economy. In: McKinsey Glob. Inst. [https://www.mckinsey.com/~media/McKinsey/Business Functions/McKinsey Digital/Our Insights/Disruptive technologies/MGI_Disruptive_technologies_Full_report_May2013.pdf](https://www.mckinsey.com/~media/McKinsey/Business%20Functions/McKinsey%20Digital/Our%20Insights/Disruptive%20technologies/MGI_Disruptive_technologies_Full_report_May2013.pdf). Accessed 16 Dec 2020
- Andó M, Birosz M, Jeganmohan S (2021) Surface bonding of additive manufactured parts from multi-colored PLA materials. *Meas J Int Meas Confed*. <https://doi.org/10.1016/j.measurement.2020.108583>
- Durgun I, Ertan R (2014) Experimental investigation of FDM process for improvement of mechanical properties and production cost. *Rapid Prototyp J*. <https://doi.org/10.1108/RPJ-10-2012-0091>
- Hassanifard S, Hashemi SM (2020) On the strain-life fatigue parameters of additive manufactured plastic materials through fused filament fabrication process. *Addit Manuf* 32:100973. <https://doi.org/10.1016/j.addma.2019.100973>
- Liu Z, Lei Q, Xing S (2019) Mechanical characteristics of wood, ceramic, metal and carbon fiber-based PLA composites fabricated by FDM. *J Mater Res Technol*. <https://doi.org/10.1016/j.jmrt.2019.06.034>
- Ehrmann G, Ehrmann A (2021) Investigation of the shape-memory properties of 3D printed pla structures with different infills. *Polymers (Basel)*. <https://doi.org/10.3390/polym13010164>
- Verbeeten WMH, Lorenzo-Bañuelos M, Arribas-Subiñas PJ (2020) Anisotropic rate-dependent mechanical behavior of Poly(Lactic Acid) processed by material extrusion additive manufacturing. *Addit Manuf* 31:100968. <https://doi.org/10.1016/j.addma.2019.100968>
- Chen JV, Dang ABC, Lee CS, Dang ABC (2019) 3D printed PLA Army-Navy retractors when used as linear retractors yield clinically acceptable tolerances. *3D Print Med* 5:16. <https://doi.org/10.1186/s41205-019-0053-z>
- Zhang X, Chen L, Mulholland T, Osswald TA (2019) Characterization of mechanical properties and fracture mode of PLA and copper/PLA composite part manufactured by fused deposition modeling. *SN Appl Sci*. <https://doi.org/10.1007/s42452-019-0639-5>
- Mohamed OA, Masood SH, Bhowmik JL (2017) Experimental investigation of time-dependent mechanical properties of PC-ABS prototypes processed by FDM additive manufacturing process. *Mater Lett*. <https://doi.org/10.1016/j.matlet.2017.01.104>
- Zhao Y, Chen Y, Zhou Y (2019) Novel mechanical models of tensile strength and elastic property of FDM AM PLA materials: Experimental and theoretical analyses. *Mater Des*. <https://doi.org/10.1016/j.matdes.2019.108089>
- Yao T, Deng Z, Zhang K, Li S (2019) A method to predict the ultimate tensile strength of 3D printing polylactic acid (PLA) materials with different printing orientations. *Compos Part B Eng*. <https://doi.org/10.1016/j.compositesb.2019.01.025>
- Zhang J, Wang P, Gao RX (2019) Deep learning-based tensile strength prediction in fused deposition modeling. *Comput Ind*. <https://doi.org/10.1016/j.compind.2019.01.011>
- Gopsill JA, Shindler J, Hicks BJ (2018) Using finite element analysis to influence the infill design of fused deposition modelled parts. *Prog Addit Manuf*. <https://doi.org/10.1007/s40964-017-0034-y>
- Alafaghani A, Qattawi A, Alrawi B, Guzman A (2017) Experimental optimization of fused deposition modelling processing parameters: a design-for-manufacturing approach. *Procedia Manuf*. <https://doi.org/10.1016/j.promfg.2017.07.079>
- Mohamed OA, Masood SH, Bhowmik JL (2016) Optimization of fused deposition modeling process parameters for dimensional accuracy using 1-optimality criterion. *Meas J Int Meas Confed*. <https://doi.org/10.1016/j.measurement.2015.12.011>
- Raut S, Jatti VS, Khedkar NK, Singh TP (2014) Investigation of the effect of built orientation on mechanical properties and total cost of FDM parts. *Procedia Mater Sci*. <https://doi.org/10.1016/j.mspro.2014.07.146>
- Carneiro OS, Silva AF, Gomes R (2015) Fused deposition modeling with polypropylene. *Mater Des*. <https://doi.org/10.1016/j.matdes.2015.06.053>
- Wu W, Geng P, Li G et al (2015) Influence of layer thickness and raster angle on the mechanical properties of 3D-printed PEEK and a comparative mechanical study between PEEK and ABS. *Materials (Basel)*. <https://doi.org/10.3390/ma8095271>
- Lanzotti A, Grasso M, Staiano G, Martorelli M (2015) The impact of process parameters on mechanical properties of parts fabricated in PLA with an open-source 3-D printer. *Rapid Prototyp J*. <https://doi.org/10.1108/RPJ-09-2014-0135>
- Alvarez CKL, Lagos CRF, Aizpun M (2016) Investigating the influence of infill percentage on the mechanical properties of fused deposition modelled ABS parts. *Ing e Investig*. <https://doi.org/10.15446/ing.investig.v36n3.56610>
- Christiyan KGJ, Chandrasekhar U, Venkateswarlu K (2016) A study on the influence of process parameters on the Mechanical Properties of 3D printed ABS composite. *IOP Conf Series Mater Sci Eng* 114:012109
- Rodríguez-Panes A, Claver J, Camacho AM (2018) The influence of manufacturing parameters on the mechanical behaviour of PLA and ABS pieces manufactured by FDM: A comparative analysis. *Materials (Basel)*. <https://doi.org/10.3390/ma11081333>
- Camargo JC, Machado ÁR, Almeida EC, Silva EFMS (2019) Mechanical properties of PLA-graphene filament for FDM 3D printing. *Int J Adv Manuf Technol*. <https://doi.org/10.1007/s00170-019-03532-5>
- Terekhina S, Skorniyakov I, Tarasova T, Egorov S (2019) Effects of the infill density on the mechanical properties of Nylon specimens made by filament fused fabrication. *Technologies*. <https://doi.org/10.3390/technologies7030057>
- Cerda-Avila SN, Medellín-Castillo HI, Lim T (2020) An experimental methodology to analyse the structural behaviour of FDM parts with variable process parameters. *Rapid Prototyp J*. <https://doi.org/10.1108/RPJ-12-2019-0312>
- Hanon MM, Marczi R, Zsidai L (2020) Influence of the 3D printing process settings on tensile strength of PLA and HT-PLA. *Period Polytech Mech Eng*. <https://doi.org/10.3311/ppme.13683>
- Gawel A, Kuciel S (2020) The study of physico-mechanical properties of polylactide composites with different level of infill produced by the fdm method. *Polymers (Basel)*. <https://doi.org/10.3390/polym12123056>

31. Medellin-Castillo HI, Zaragoza-Siqueiros J (2019) Design and manufacturing strategies for fused deposition modelling in additive manufacturing: a review. *Chinese J Mech Eng (English Ed)*. <https://doi.org/10.1186/s10033-019-0368-0>
32. Rezaie R, Badrossamay M, Ghaei A, Moosavi H (2013) Topology optimization for fused deposition modeling process. *Procedia CIRP* 6:521–526
33. Mostafa KG, Montemagno C, Qureshi AJ (2018) Strength to cost ratio analysis of FDM Nylon 12 3D printed parts. *Procedia Manuf* 26:753–762
34. Al-Ghamdi KA (2019) Sustainable FDM additive manufacturing of ABS components with emphasis on energy minimized and time efficient lightweight construction. *Int J Light Mater Manuf*. <https://doi.org/10.1016/j.ijlmm.2019.05.004>
35. Kousiatza C, Karalekas D (2016) In-situ monitoring of strain and temperature distributions during fused deposition modeling process. *Mater Des*. <https://doi.org/10.1016/j.matdes.2016.02.099>
36. Zhang W, Wu AS, Sun J et al (2017) Characterization of residual stress and deformation in additively manufactured ABS polymer and composite specimens. *Compos Sci Technol*. <https://doi.org/10.1016/j.compscitech.2017.07.017>
37. Courter B, Savane V, Bi J et al (2017) Finite element simulation of the fused deposition modelling process. In: *Proceedings of the NAFEMS World Congress*. Stockholm, Sweden
38. Sunny S, Chen H, Malik A, Lu H (2020) Influence of residual stress and fluid–structure interaction on the impact behavior of fused filament fabrication components. *Addit Manuf*. <https://doi.org/10.1016/j.addma.2020.101662>
39. Deswal S, Narang R, Chhabra D (2019) Modeling and parametric optimization of FDM 3D printing process using hybrid techniques for enhancing dimensional preciseness. *Int J Interact Des Manuf*. <https://doi.org/10.1007/s12008-019-00536-z>
40. Kantaros A, Karalekas D (2013) Fiber Bragg grating based investigation of residual strains in ABS parts fabricated by fused deposition modeling process. *Mater Des*. <https://doi.org/10.1016/j.matdes.2013.02.067>
41. Casavola C, Cazzato A, Moramarco V, Pappalettera G (2017) Residual stress measurement in fused deposition modelling parts. *Polym Test*. <https://doi.org/10.1016/j.polymertesting.2017.01.003>
42. Tronvoll SA, Welo T, Elverum CW (2018) The effects of voids on structural properties of fused deposition modelled parts: a probabilistic approach. *Int J Adv Manuf Technol*. <https://doi.org/10.1007/s00170-018-2148-x>
43. Webbe Kerekes T, Lim H, Joe WY, Yun GJ (2019) Characterization of process–deformation/damage property relationship of fused deposition modeling (FDM) 3D-printed specimens. *Addit Manuf* 25:532–544. <https://doi.org/10.1016/J.ADDMA.2018.11.008>
44. Samykano M, Selvamani SK, Kadirgama K et al (2019) Mechanical property of FDM printed ABS: influence of printing parameters. *Int J Adv Manuf Technol*. <https://doi.org/10.1007/s00170-019-03313-0>
45. Abeykoon C, Sri-Amphorn P, Fernando A (2020) Optimization of fused deposition modeling parameters for improved PLA and ABS 3D printed structures. *Int J Light Mater Manuf*. <https://doi.org/10.1016/j.ijlmm.2020.03.003>
46. Serdeczny MP, Comminal R, Mollah MT et al (2020) Numerical modeling of the polymer flow through the hot-end in filament-based material extrusion additive manufacturing. *Addit Manuf*. <https://doi.org/10.1016/j.addma.2020.101454>
47. Rajpurohit SR, Dave HK (2019) Analysis of tensile strength of a fused filament fabricated PLA part using an open-source 3D printer. *Int J Adv Manuf Technol*. <https://doi.org/10.1007/s00170-018-3047-x>
48. Peng A, Xiao X, Yue R (2014) Process parameter optimization for fused deposition modeling using response surface methodology combined with fuzzy inference system. *Int J Adv Manuf Technol*. <https://doi.org/10.1007/s00170-014-5796-5>
49. Padhi SK, Sahu RK, Mahapatra SS et al (2017) Optimization of fused deposition modeling process parameters using a fuzzy inference system coupled with Taguchi philosophy. *Adv Manuf*. <https://doi.org/10.1007/s40436-017-0187-4>
50. Huynh HN, Nguyen AT, Ha NL, Ha Thai TT (2017) Application of fuzzy Taguchi method to improve the dimensional accuracy of fused deposition modeling processed product. In: *Proceedings-2017 International Conference on System Science and Engineering, ICSSE 2017*

Publisher's Note Springer Nature remains neutral with regard to jurisdictional claims in published maps and institutional affiliations.